Journal of Earth Science, *Vol. 27*, *No. 3*, *p. 474–490*, *June 2016* *ISSN 1674-487X*
Printed in China
DOI: 10.1007/s12583-016-0674-6

Geochronology and Petrogenesis of Triassic High-K Calc-Alkaline Granodiorites in the East Kunlun Orogen, West China: Juvenile Lower Crustal Melting during Post-Collisional Extension

Fuhao Xiong[1, 2], **Changqian Ma***[3], **Hong'an Jiang**[4], **Hang Zhang**[3]

1. *Key Laboratory of Tectonic Controls on Mineralization and Hydrocarbon Accumulation*, *Ministry of Land and Resources*, *College of Earth Sciences*, *Chengdu University of Technology*, *Chengdu* 610059, *China*
2. *State Key Laboratory of Continental Tectonics and Dynamics*, *Institute of Geology*, *Chinese Academy of Geological Sciences*, *Beijing* 100037, *China*
3. *State Key Laboratory of Geological Processes and Mineral Resources*, *China University of Geosciences*, *Wuhan* 430074, *China*
4. *Changsha Uranium Geology Research Institute*, *CNNC*, *Changsha* 410007, *China*

ABSTRACT: This study reports zircon U-Pb and Hf isotopes and whole-rock elemental data for granodiorites from the East Kunlun orogen. The zircon U-Pb dating defines their crystallization age of 235 Ma. The rocks are characterized by high-K calc-alkaline, magnesian and metaluminous with (K_2O+Na_2O)=6.38 wt.%–7.01 wt.%, Mg#=42–50 [Mg#=100×molar Mg/(Mg+FeO^T)], A/CNK=0.92–0.98, coupled with high $\varepsilon_{Hf}(t)$ values from -0.65 to -1.80. The rocks were derived from partial melting of a juvenile mafic crustal source within normal crust thickness. The juvenile lower crust was generated by mixing lithospheric mantle-derived melt (55%–60%) and supracrustal melt (40%–45%) during the seafloor subduction. Together with available data from the East Kunlun, it is proposed that the studied Middle Triassic granodiorites were formed in post-collisional extension setting, in which melting of the juvenile lower crust in response to the basaltic magma underplating resulted in the production of high-K granodioritic melts.

KEY WORDS: East Kunlun, granodiorite, geochronology, Hf isotope, magmatism.

0 INTRODUCTION

Orogenic belts, widely distributed in the Qinghai-Tibet Plateau, are the pivotal sites for better understanding of the theory of crustal growth and the orogenic evolution on the Earth, since they have experienced multiple episodic tectono-magmatic cycles during the eastern Tethyan orogeny (Xiong et al., 2014; Xu et al., 2014; Bouilhol et al., 2013; Mo et al., 2009; Yang et al., 2009). As the most typical product of orogeny, granitoids can provide valuable geodynamic information on the crustal growth and the tectonic evolution, because their geochemical and isotopic compositions can constrain the nature of source and the conditions of magma origin (Bellos et al., 2015; Bergemann et al., 2014; Gong et al., 2014; Ostendorf et al., 2014).

In this study, we focus on the granitoids in the East Kunlun orogenic belt (EKOB), which is the typical Tethyan orogenic belt in the Qinghai-Tibet Plateau. The granitoids in the EKOB mostly comprise Triassic high-K calc-alkaline rocks (Chen et al., 2015; Xiong et al., 2014; Zhang et al., 2012), which are typical but genetic complex rocks in the Earth. The high-K calc-alkaline granitoids generally show arc-related geochemical imprints, which are however not necessarily explained as they were generated in subduction zone (Castro, 2014; Pitcher, 1987), collisional or extensional settings are also reasonable alternatives (Honarmand et al., 2015; Eyal et al., 2010; Ajaji et al., 1998). The AFC (assimilation-fractional crystallization) processes of basaltic magmas, partial melting of mafic to intermediate igneous sources and crust-mantle interaction are possibilities to produce such magmas (Simon et al., 2014; Cocherie et al., 1994; Rapp et al., 1991). Obviously, rationally determining the petrogenesis and tectonic implications of high-K calc-alkaline granitoids is the key to understanding the crustal growth and tectonic evolution of the EKOB. In this study, new zircon U-Pb and Hf isotopes and whole-rock elemental data for the Triassic granodiorites are used to quantify the origin of the studied rocks, with the purpose of providing additional insights into mantle-crust interactions and the petrogenesis of high-K calc-alkaline felsic magmas.

1 GEOLOGICAL SETTING

The EKOB makes up the north part of the Qinghai-Tibetan Plateau (Fig. 1a), which is located between the Qaidam Basin to the north and the Bayan Har terrane to the south (Fig. 1a). It is widely accepted that the EKOB represents the boundary

*Corresponding author: cqma@cug.edu.cn

Manuscript received July 10, 2015.
Manuscript accepted November 1, 2015.

Xiong, F. H., Ma, C. Q., Jiang, H. A., et al., 2016. Geochronology and Petrogenesis of Triassic High-K Calc-Alkaline Granodiorites in the East Kunlun Orogen, West China: Juvenile Lower Crustal Melting during Post-Collisional Extension. *Journal of Earth Science*, 27(3): 474–490. doi:10.1007/s12583-016-0674-6. http://en.earth-science.net

between the Gondwana land and Laurasia domains after the subduction of the Paleo-Tethyan Ocean (Yang et al., 2009, 1996). Subduction of the oceanic plate and subsequent continental collision resulted in the occurrence of large-scale granitic magmatism in the EKOB during Late Permian to Late Triassic (Fig. 1b) (Xiong et al., 2014, 2013; Zhang et al., 2012).

The basement rocks of the studied area are the Proterozoic Xiaomiao Formation, consisting of two parts, i.e., the lower part of marble, amphibolite and biotite-hornblende gneiss, and the upper part of mica quartz schist, marble and metagreywacke. Unconformably overlying the Xiaomiao Formation are Ordovician marine clastic and carbonate formation. Silurian–Middle Devonian strata are missing because the terrane uplifted at that time, but Late Devonian strata are present consisting of continental volcanic rocks. During Early Carboniferous to Permian, the area mainly consisted of shallow marine and paralic clastic formations (Bian et al., 2004). Oceanic subduction and continental collision took place during the Early Triassic, which led to the occurrence of widespread fold-thrust deformation and granitic magmatism in the EKOB (Xiong et al., 2014, 2012; Xu et al., 2001).

The studied granitic pluton, showing sharp contacts with their wall-rocks, intrudes into the Mesozoic strata (Fig. 1b) and is located in the eastern section of EKOB.

2 SAMPLING AND PETROGRAPHY

The samples for dating and geochemistry analyses are shown in Fig. 1c. The main lithology of the pluton is granodiorite, with small amount of porphyritic granodiorite (Fig. 2). The granitic pluton intrudes into the Early Triassic strata, and is characterized by development of joints (Fig. 2a).

The granodiorites are medium-grained, massive, and equigranular (Fig. 2b), consisting of plagioclase (40 vol.%–45 vol.%), quartz (20 vol.%–25 vol.%), K-feldspar (10 vol.%–15 vol.%), hornblende (5 vol.%–10 vol.%) and biotite (~5 vol.%). The accessory minerals are titanite, apatite, zircon, epidote and opaques. The local visible porphyritic granodiorites are medium-grained and porphyraceous (Fig. 2c) with large phenocrysts (length up to 5 mm) of plagioclase (5 vol.%–10 vol.%) and minor amounts of K-feldspar. The groundmass is fine-

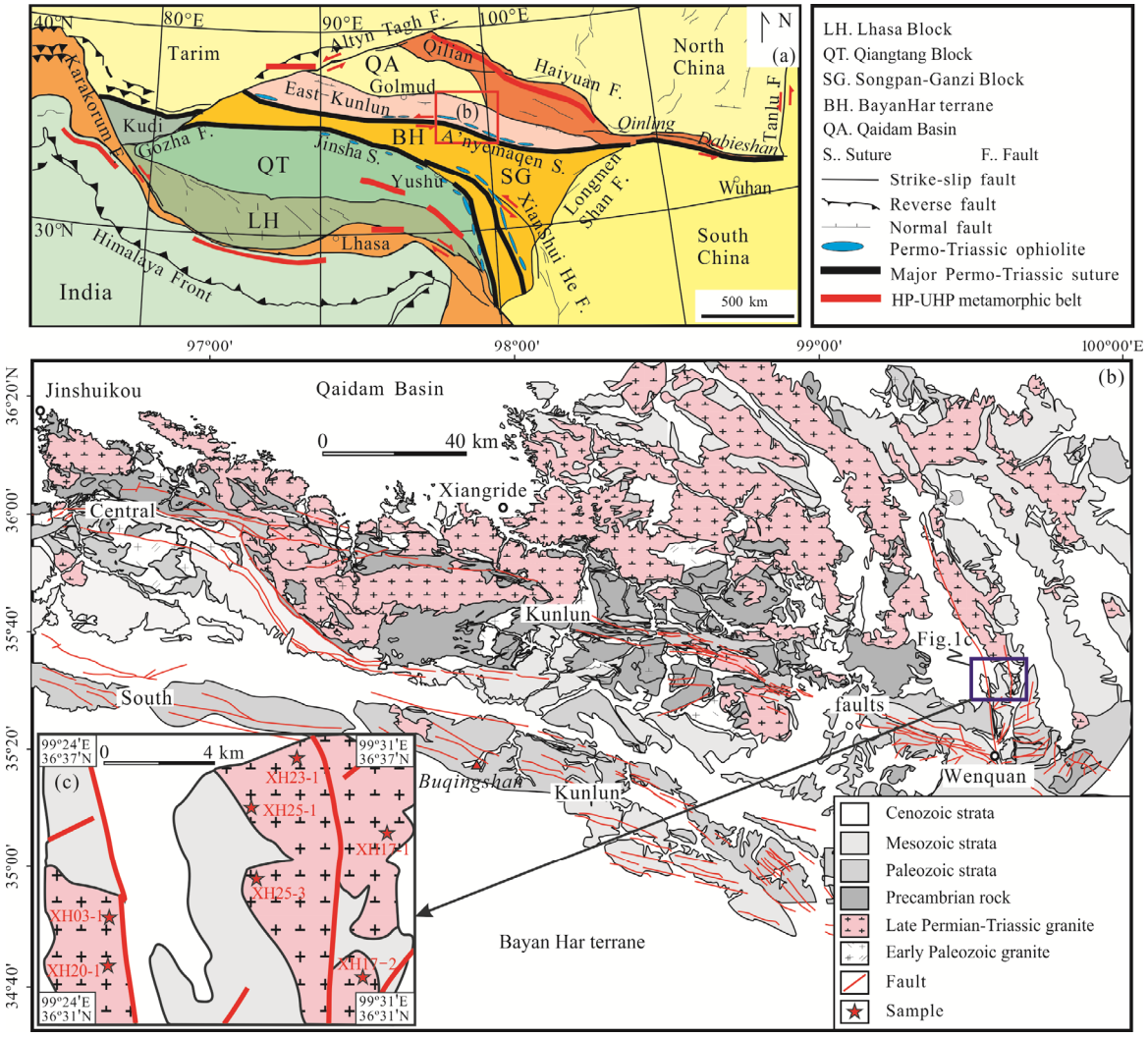

Figure 1. (a) Tectonic outline of the Tibetan Plateau showing the location of the EKOB (modified from Roger et al., 2003); (b) simplified geological map showing the distribution of granitoids in the EKOB (after Xiong et al., 2014); (c) simplified geological map of the studied granodioritic pluton.

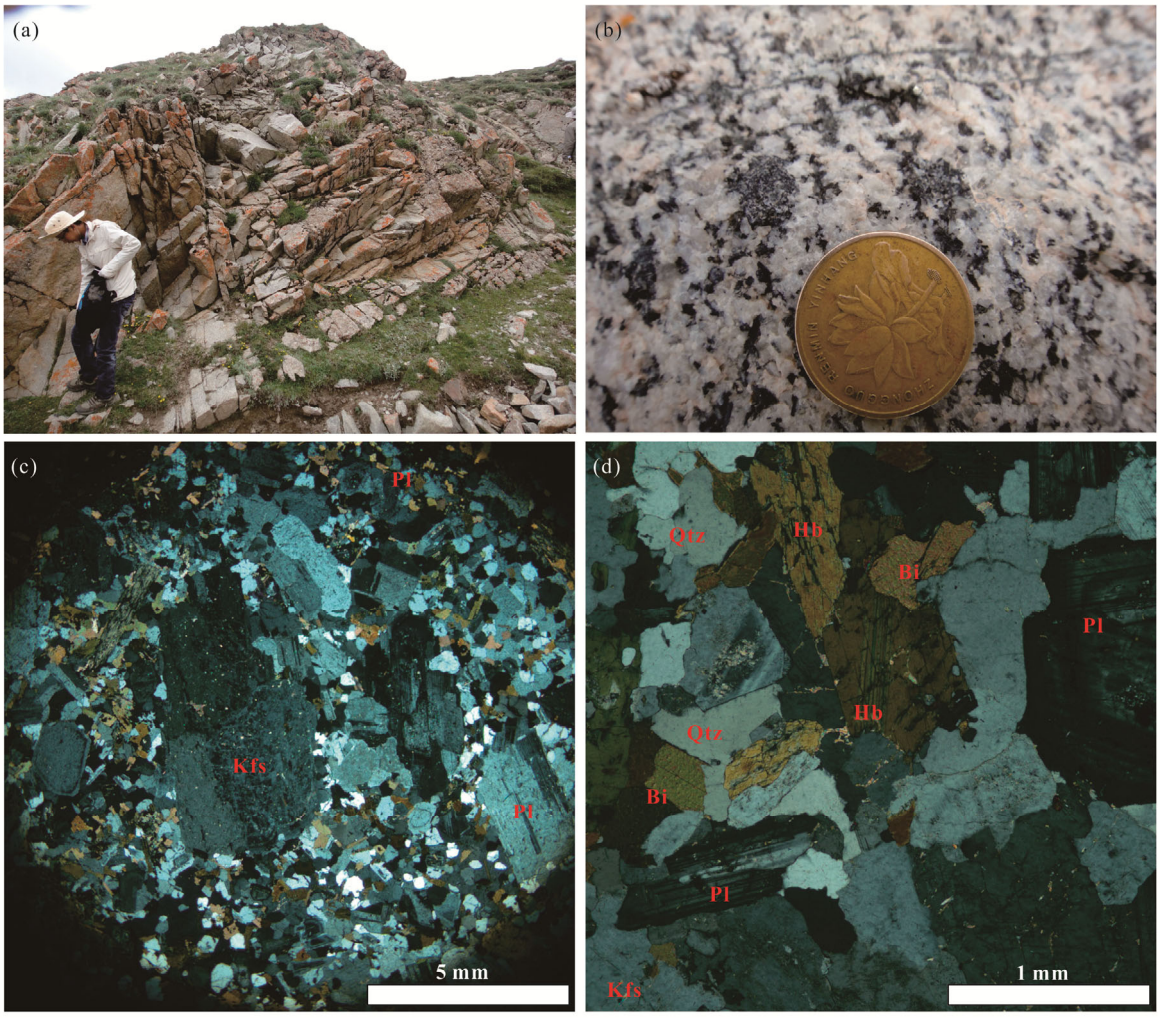

Figure 2. Field and thin section photographs showing the studied granodiorites in the East Kunlun orogen. (a) and (b) the granodiorites show joint structure and equigranular texture; (c) the local visible porphyritic granodiorites showing porphyritic texture; (d) the granodiorites exhibiting equigranular texture dominated by plagioclase, quartz, potassium feldspar, amphibole and biotite.

grained, consisting of plagioclase (40 vol.%–45 vol.%), quartz (20 vol.%–25 vol.%), K-feldspar (10 vol.%–15 vol.%), hornblende (~5 vol.%) and biotite (~5 vol.%).

3 ANALYTICAL METHODS

The samples collected from fresh outcrops were separated for zircons by heavy-liquid and magnetic methods. Zircon grains were photographed with an optical microscope, and their internal structure was checked by cathodoluminescence (CL). The U-Pb dating was done by laser ablation-inductively coupled plasma-mass spectrometry (LA-ICP-MS) at the State Key Laboratory of Geological Processes and Mineral Resources (GPMR), China University of Geosciences, Wuhan. Zircon 91500 was used as external standard for U-Pb dating, and was analyzed twice every 5 analyses, the laser beam spot was 32 μm. Laser sampling was performed using a GeoLas 2005. An Agilent 7500a ICP-MS instrument was used to acquire ion-signal intensities. Helium was applied as carrier gas. Argon was used as the make-up gas and mixed with the carrier gas via a T-connector before entering the ICP. Nitrogen was added into the central gas flow (Ar+He) of the Ar plasma to lower the detection limit and improve precision. Concordia diagrams and weighted mean calculations were made using Isoplot/Ex_ver3 (Ludwig, 2003). Data were processed by ICPMSDataCal (Liu et al., 2010). Detailed operating conditions for the laser ablation system and the ICP-MS instrument are the same as described by Liu et al. (2010).

Whole rock samples were crushed in a corundum jaw crusher (to 60 meshes). About 60 g was powdered in an agate ring mill to less than 200 meshes for whole rock geochemistry analysis. Whole rock major element analyses were conducted by a Rigaku 3080E1-type spectrometer XRF at the Bureau of Geology and Mineral Resources, Hubei Province, China, with analytical precision better than 5%. Trace elements were analyzed with an Agilent 7500a ICP-MS at GPMR Laboratory, China University of Geosciences, Wuhan. The detailed sample-digesting procedure for ICP-MS analyses, analytical precision and accuracy for trace elements are the same as described by Liu et al. (2010).

In-situ Hf isotope ratio analysis of zircon was conducted on the dated zircon grains using a Neptune Plus MC-ICP-MS (Thermo Fisher Scientific, Germany) in combination with a

Geolas 2005 excimer ArF laser ablation system (Lambda Physik, Göttingen, Germany) that was hosted at the GPMR, China University of Geosciences in Wuhan. All data were acquired on zircon in single spot ablation mode at a spot size of 44 μm. Detailed operating conditions for the laser ablation system and the MC-ICP-MS instrument and analytical method are the same as described by Hu et al. (2012). Off-line selection and integration of analytical signals, and mass bias calibrations were performed using ICPMSDataCal (Liu et al., 2010).

4 RESULTS

4.1 LA-ICP-MS U-Pb Zircon Dating

Zircon U-Pb data are presented in Table 1. Zircons from granodiorites are 200 to 300 μm in the longest dimension, with width/length ratios of about 1 : 2 to 1 : 5. All the zircons are transparent or pale yellow, euhedral columnar crystals, without inclusions and very limpid. Zircons from samples XH23-1 and XH03-1 exhibit typical oscillatory zoning (Fig. 3). The zircons have high concentrations of Th and U (Table 1) and large Th/U ratios (0.48–0.85 and 0.27–0.58, respectively), indicative of magmatic origin (Corfu et al., 2003; Hoskin and Schaltegger, 2003).

Zircons from Sample XH23-1 have high Th and U contents (Th=366 ppm–1 059 ppm, U=598 ppm–1 805 ppm) and high ratios of Th/U (average=0.59). Twenty spots were analyzed, which yield concordant $^{206}Pb/^{238}U$ ages ranging from 231 to 239 Ma (Table 1). The analyses give a weighted mean age of 235.4±1.5 Ma (MSWD=0.21, 1σ for errors), which is identical to the concordant age (235.5±1.6 Ma, Fig. 3).

Zircons from Sample XH03-1 have similar contents of Th and U to those from Sample XH23-1 (Th=219 ppm–1 174 ppm, U=809 ppm–2 441 ppm, Table 1) and similar ratios of Th/U (average=0.48). Twenty spots were analyzed, and the zircons yield similar $^{206}Pb/^{238}U$ ages ranging from 228 to 243 Ma, and give a weighted mean of 234.5±1.9 Ma (MSWD=1.8, 1σ for errors), which is similar, within error, to their concordant age (232.2±1.8 Ma, Fig. 3). Thus, the best estimate for the crystallization age of the granodiorite may be ca. 235 Ma, which represents the granitic magmatism occurred at Middle Triassic.

4.2 Whole-Rock Geochemistry

Selected chemical analysis of representative samples are listed in Table 2. The granodiorites span a narrow range of SiO_2 content (63.60 wt.%–67.00 wt.%), and define a subalkaline trend in the total alkali-silica (TAS) diagram (Fig. 4a). The granodiorites have moderate concentations of FeO^T (3.24 wt.%–4.66 wt.%) and MgO (1.67 wt.%–2.39 wt.%), with high values of Mg# [Mg#=100×molar Mg/(Mg+ FeO^T); 42–50], showing characteristics of magnesian granitoids (Fig. 4b). The granodiorites have high contents of K_2O+Na_2O (6.38 wt.%–

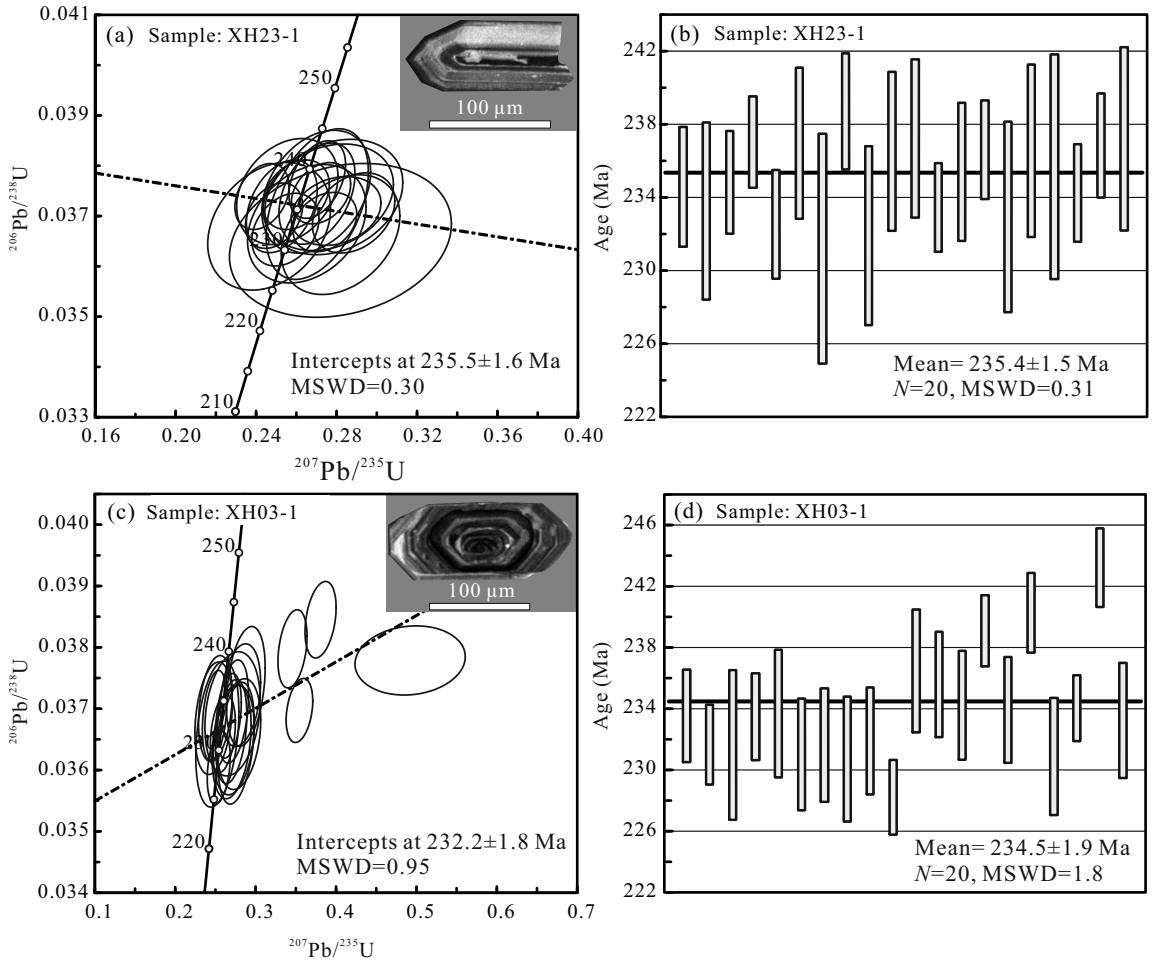

Figure 3. Representative CL images of zircons and Zircon U-Pb concordia diagrams for the studied granodiorites in the East Kunlun.

Table 1 Zircon U-Pb data for the studied granodiorites in the East Kunlun orogen

Analysis	Contents		Ratios	Isotopic ratios						Isotopic ages (Ma)					
	Th	U	Th/U	$^{207}Pb/^{206}Pb$	1σ	$^{207}Pb/^{235}U$	1σ	$^{206}Pb/^{238}U$	1σ	$^{207}Pb/^{206}Pb$	1σ	$^{207}Pb/^{235}U$	1σ	$^{206}Pb/^{238}U$	1σ
XH03-1															
01	961	2 14 9	0.45	0.048 8	0.002 0	0.249 0	0.010 1	0.036 9	0.000 5	200	98	226	8	234	3
02	1 025	2 01 2	0.51	0.051 3	0.002 2	0.259 2	0.010 3	0.036 6	0.000 4	254	98	234	8	232	3
03	219	809	0.27	0.050 0	0.003 5	0.252 4	0.017 7	0.036 6	0.000 8	195	158	229	14	232	5
04	804	1 821	0.44	0.052 3	0.002 2	0.266 4	0.010 4	0.036 9	0.000 5	302	90	240	8	233	3
05	642	1 438	0.45	0.053 3	0.004 8	0.271 3	0.022 7	0.036 9	0.000 7	343	204	244	18	234	4
06	731	1 604	0.46	0.054 5	0.003 8	0.272 7	0.016 7	0.036 5	0.000 6	391	156	245	13	231	4
07	737	1 478	0.50	0.055 9	0.004 2	0.279 4	0.017 8	0.036 6	0.000 6	450	167	250	14	232	4
08	985	1 956	0.50	0.054 6	0.003 0	0.275 8	0.014 9	0.036 4	0.000 7	398	92	247	12	231	4
09	954	2 064	0.46	0.053 6	0.002 9	0.269 6	0.012 8	0.036 6	0.000 6	354	123	242	10	232	3
10	864	1 868	0.46	0.051 0	0.001 9	0.254 1	0.009 4	0.036 0	0.000 4	243	87	230	8	228	2
11	794	1 821	0.44	0.055 6	0.003 1	0.287 7	0.015 9	0.037 4	0.000 6	435	131	257	13	236	4
12	1 174	2 026	0.58	0.054 4	0.003 2	0.281 3	0.016 5	0.037 2	0.000 6	387	133	252	13	236	3
13	852	1 530	0.56	0.048 8	0.002 8	0.249 9	0.013 8	0.037 0	0.000 6	139	194	227	11	234	4
14	1 167	2 441	0.48	0.094 3	0.009 3	0.492 2	0.045 3	0.037 8	0.000 4	1 515	187	406	31	239	2
15	1 123	2 074	0.54	0.052 8	0.002 5	0.271 8	0.012 7	0.037 0	0.000 6	320	112	244	10	234	3
16	1 034	2 005	0.52	0.065 5	0.002 4	0.345 9	0.011 9	0.038 0	0.000 4	791	71	302	9	240	3
17	1 022	2 033	0.50	0.053 4	0.003 3	0.270 2	0.016 0	0.036 5	0.000 6	346	134	243	13	231	4
18	876	1 767	0.50	0.068 9	0.002 1	0.354 5	0.010 9	0.037 0	0.000 3	898	65	308	8	234	2
19	926	1 631	0.57	0.071 8	0.002 4	0.380 8	0.012 8	0.038 5	0.000 4	989	73	328	9	243	3
20	700	1 345	0.52	0.048 8	0.003 3	0.247 8	0.015 4	0.036 8	0.000 6	200	87	225	13	233	4

Table 1 Continued

Analysis	Contents		Ratios	Isotopic ratios						Isotopic ages (Ma)					
	Th	U	Th/U	$^{207}Pb/^{206}Pb$	1σ	$^{207}Pb/^{235}U$	1σ	$^{206}Pb/^{238}U$	1σ	$^{207}Pb/^{206}Pb$	1σ	$^{207}Pb/^{235}U$	1σ	$^{206}Pb/^{238}U$	1σ
XH23-1															
01	945	1 243	0.76	0.056 6	0.002 8	0.288 5	0.013 5	0.037 1	0.000 5	476	111	257	11	235	3
02	747	1 010	0.74	0.052 5	0.004 1	0.265 2	0.019 5	0.036 8	0.000 8	306	180	239	16	233	5
03	518	874	0.59	0.054 6	0.002 9	0.279 7	0.014 8	0.037 1	0.000 5	394	119	250	12	235	3
04	770	1 359	0.57	0.053 1	0.002 0	0.272 3	0.009 7	0.037 5	0.000 4	332	79	245	8	237	2
05	550	1 073	0.51	0.051 0	0.002 3	0.254 6	0.011 0	0.036 7	0.000 5	243	106	230	9	233	3
06	986	1 163	0.85	0.052 9	0.002 6	0.270 3	0.012 5	0.037 4	0.000 7	324	111	243	10	237	4
07	377	705	0.53	0.058 4	0.008 5	0.282 0	0.036 4	0.036 5	0.001 0	546	321	252	29	231	6
08	905	1 362	0.66	0.052 4	0.001 9	0.270 4	0.009 3	0.037 7	0.000 5	306	81	243	7	239	3
09	932	1 394	0.67	0.055 7	0.003 8	0.282 0	0.019 5	0.036 6	0.000 8	439	154	252	15	232	5
10	628	1 101	0.57	0.053 6	0.004 3	0.275 9	0.021 4	0.037 4	0.000 7	354	180	247	17	237	4
11	496	904	0.55	0.049 6	0.003 2	0.255 5	0.016 6	0.037 5	0.000 7	176	150	231	13	237	4
12	615	1 272	0.48	0.053 4	0.002 0	0.274 2	0.010 5	0.036 9	0.000 4	346	85	246	8	233	2
13	932	1 480	0.63	0.049 1	0.002 3	0.252 8	0.011 6	0.037 2	0.000 6	154	111	229	9	235	4
14	601	1 255	0.48	0.047 6	0.001 9	0.242 9	0.008 9	0.037 4	0.000 4	79.7	92.6	221	7	237	3
15	366	598	0.61	0.048 2	0.004 0	0.246 5	0.020 2	0.036 8	0.000 8	109	185	224	16	233	5
16	370	679	0.55	0.053 9	0.004 5	0.278 6	0.022 6	0.037 4	0.000 8	369	187	250	18	237	5
17	698	1 381	0.51	0.052 9	0.003 6	0.270 4	0.016 8	0.037 2	0.001 0	324	153	243	13	236	6
18	1 058	1 805	0.59	0.048 2	0.001 8	0.248 9	0.009 4	0.037 0	0.000 4	109	87	226	8	234	3
19	611	1 240	0.49	0.050 4	0.002 2	0.259 9	0.010 9	0.037 4	0.000 5	213	106	235	9	237	3
20	651	1 203	0.54	0.052 3	0.003 7	0.269 9	0.017 8	0.037 5	0.000 8	302	161	243	14	237	5

7.01 wt.%), moderate contents of CaO (3.63 wt.%–4.24 wt.%), showing calc-alkaline trend (Fig. 4c). All the rocks are metaluminous (A/CNK=0.92–0.98; Fig. 4d), resembling typical I-type granitoids (Chappell and White, 2001; Chappell, 1999).

In the chondrite-normalized REE diagrams (Fig. 5a), the granodiorites exhibit enrichment of light rare earth elements (LREE) with $(La/Yb)_N$ of 9.05–21.90, and show moderate negative Eu anomalies (δEu=0.68–0.84), as well as higher differentiation of LREEs [$(La/Sm)_N$=4.15–5.07] than those of heavy rare earth elements (HREE) [$(Gd/Yb)_N$=1.52–2.73; Fig. 5a]. All the rocks are characterized by depletion of Nb, Ta, P, and Ti, and strong enrichment of large ion lithophile elements (LILE) in the primitive mantle-normalized trace element spider diagram (Fig. 5b).

4.3 Zircon Lu-Hf Isotopic Compositions

Zircons from the granodiorite (XH23-1) with $^{206}Pb/^{238}U$ age of 235 Ma have high initial $^{176}Hf/^{177}Hf$ values [$(^{176}Hf/^{177}Hf)_i$=0.282 577–0.282 610, Table 3], and display homogeneous isotopic compositions with $\varepsilon_{Hf}(t)$ values ranging from -1.80 to -0.65. Two-stage model ages (T_{2DM}) are calculated by assuming a mean $^{176}Lu/^{177}Hf$ value of 0.015 for an average continental crust (Griffin et al., 2002), and the zircons from the studied rocks have similar two-stage Hf model ages of 1.31–1.38 Ga.

5 DISCUSSION

5.1 Petrogenesis of the Granodiorites

5.1.1 Source type and magmatic processes

Several models have been proposed to account for the generation of calc-alkaline granodioritic magmas. Two large model categories are distinguished depending on the locus of magma generation: (1) those invoking fractional crystallization of a mantle-derived basaltic parent magma (Castro, 2013; Soesoo, 2000), which may further assimilate crustal materials to account for their trace elements and isotopic enrichment (Depaolo, 1981), and (2) those invoking remelting of a lower crust basaltic protolith (Jagoutz et al., 2013; Jung et al., 2009). Contemporaneous basaltic magma in the EKOB is alkaline and has Hf-Nd isotopes identical to the OIB (Hu et al., 2015; Xiong et al., 2013), arguing against the studied granodioritic magma was formed by extensive fractionation of basaltic magma. The absence of gabbro-diorite-granodiorite suites in the studied area also argues against the fractionation of basaltic magma, because fractionation of basaltic magma would produce dioritic, tonalitic, granodioritic, and granitic melts which constrain the liquid line of descent (Bucholz et al., 2014; Castro, 2013).

Instead we favour a model invoking partial melting of a mafic protolith in the post-collisional setting, to generate the granodioritic magma. The studied granodiorites have low SiO_2 (63.6 wt.%–67.0 wt.%), suggesting one mafic source such as amphibolite. Hydrous melting of a mafic source generally generates a peraluminous melt (Beard et al., 2004). The studied granodiorites are metaluminous with A/CNK values of 0.92–0.99 (Table 2), indicating water-unsaturated partial melting. Dehydration melting experiments of mafic protolith at lower crustal temperatures (800–1 000 ºC) and pressure (6.9 kbar) generates metaluminous granodioritic to trondhjemitic melts (Rapp and Watson, 1995; Beard and Lofgren, 1991) similar to the studied rocks. The potassium contents of the silicic melts generated by dehydration melting of mafic protolith are chiefly controlled by the initial potassium contents of their sources (Sisson et al., 2004). Thus, the average composition of the mafic lower crust would have a high-K composition appropriate for the source of the granodioritic magma.

Table 2 Whole-rock geochemical compositions of the studied granodiorites in East Kunlun orogenic belt

Samples	XH03-1	XH17-1	XH17-2	XH20-1	XH23-1	XH25-1	XH25-3
Major element (wt.%)							
SiO_2	63.60	65.76	64.66	67.00	65.98	66.13	66.52
TiO_2	0.55	0.63	0.61	0.53	0.57	0.52	0.55
Al_2O_3	15.80	15.42	15.53	15.75	15.44	15.55	15.10
Fe_2O_3	0.62	1.20	1.25	0.62	1.56	1.20	1.69
FeO	4.10	2.92	3.10	2.68	2.85	3.03	2.80
MnO	0.05	0.07	0.07	0.06	0.08	0.08	0.09
MgO	2.29	2.06	2.39	1.67	1.74	1.77	1.76
CaO	4.24	3.82	4.12	3.77	3.80	3.78	3.63
Na_2O	2.33	3.46	3.41	3.76	3.74	3.79	3.67
K_2O	4.05	3.55	3.52	2.82	2.98	2.99	3.09
P_2O_5	0.13	0.14	0.13	0.12	0.12	0.10	0.12
LOI	1.73	0.47	0.66	0.68	0.61	0.49	0.52
Total	99.49	99.50	99.45	99.46	99.47	99.43	99.54
FeO^T	4.66	4.00	4.22	3.24	4.25	4.11	4.32
Mg#	47	48	50	48	42	43	42

Table 2 Continued

Samples	XH03-1	XH17-1	XH17-2	XH20-1	XH23-1	XH25-1	XH25-3
Trace element (ppm)							
V	55.8	62.2	69.8	51.3	67.8	67.1	67.3
Sc	9.36	8.85	9.92	6.65	9.38	10.1	10.1
Cr	45.7	28.5	33.9	23.8	9.69	11.4	10.6
Co	9.77	10.2	11.2	7.54	9.88	10.4	10.3
Ni	15.1	11.5	12.7	6.27	4.72	4.90	4.58
Zn	91.4	57.3	56.2	54.9	59.4	59.9	59.6
Cu	96.9	6.16	8.60	1.56	3.63	4.08	3.21
Ga	18.6	18.8	18.0	19.6	18.0	18.3	18.0
Rb	164	153	141	82.1	106	120	121
Sr	403	373	367	523	315	307	278
Y	15.9	20.4	21.5	13.1	22.4	23.8	24.7
Zr	156	210	207	154	132	177	222
Nb	11.1	12.6	11.7	9.70	11.2	10.7	12.0
Cs	4.85	6.10	5.77	2.07	3.29	3.98	4.66
Ba	757	775	827	923	863	834	830
Hf	4.38	5.64	5.66	4.29	3.89	4.86	6.12
Ta	0.94	1.11	0.99	0.88	0.76	0.85	0.93
Pb	7.90	22.4	19.5	15.3	14.9	16.7	17.3
Th	13.4	23.2	19.6	10.7	11.9	15.7	14.9
U	3.67	2.43	2.45	2.29	1.17	2.19	1.59
La	34.4	41.9	38.7	34.1	29.0	38.2	34.3
Ce	63.4	81.4	78.1	63.3	53.4	70.8	63.6
Pr	7.01	8.66	8.35	7.00	6.05	7.68	6.95
Nd	24.7	31.1	29.9	25.2	22.6	27.1	25.7
Sm	4.27	5.27	5.40	4.33	4.40	4.97	4.84
Eu	1.11	1.13	1.10	1.08	1.11	1.11	1.07
Gd	3.63	4.55	4.58	3.54	4.12	4.39	4.60
Tb	0.54	0.67	0.68	0.48	0.64	0.68	0.72
Dy	2.86	3.69	3.70	2.60	3.93	3.98	4.16
Ho	0.55	0.70	0.75	0.46	0.79	0.83	0.85
Er	1.51	1.96	2.10	1.22	2.18	2.40	2.44
Tm	0.23	0.28	0.33	0.18	0.35	0.36	0.38
Yb	1.39	1.86	1.94	1.05	2.16	2.35	2.41
Lu	0.23	0.28	0.32	0.17	0.33	0.39	0.39
∑REE	162	204	198	158	153	189	177
$(La/Yb)_N$	16.7	15.2	13.5	21.9	9.05	11.0	9.63
$(Gd/Yb)_N$	2.11	1.98	1.91	2.73	1.55	1.52	1.55
δEu	0.84	0.69	0.66	0.82	0.79	0.71	0.68

Note: Total Fe as FeO^T; Mg#=100×molar MgO/(MgO+FeO^T).

Besides, the major-element geochemical variation also further indicates that the magma was generated from the water undersaturated source at a low pressure condition (Fig. 6) (Castro, 2013). The inference of low pressure source is in agreement with the REE patterns of the studied granodiorites. The experimental studies show that garnet would be major residual phases at a high pressure (8–11 kbar) (Wyllie and Wolf, 1993). If garnet is a residual phase in the source, the resultant magmas would show strong HREE depletion. Thus, the possibility of a high pressure magma source can be excluded because of the studied rocks show flat HREE patterns and high HREE concentrations (Fig. 5a). If amphibole is a residual phase,

Table 3 Zircon Lu-Hf isotopic compositions from the studied granodiorites in the East Kunlun orogenic belt

Sample	$^{176}Yb/^{177}Hf$	1σ	$^{176}Lu/^{177}Hf$	1σ	$^{176}Hf/^{177}Hf$	1σ	T_{DM1} (Ga)	T_{DM2} (Ga)	$(^{176}Hf/^{177}Hf)_i$	$\varepsilon_{Hf}(t)$	1σ	$f_{Lu/Hf}$
XH23-1												
01	0.038 687	0.001 404	0.001 376	0.000 043	0.282 605	0.000 009	0.93	1.33	0.282 599	-1.01	0.33	-0.96
02	0.031 222	0.001 249	0.001 082	0.000 042	0.282 597	0.000 009	0.93	1.35	0.282 593	-1.25	0.33	-0.97
03	0.040 073	0.001 020	0.001 384	0.000 031	0.282 595	0.000 009	0.94	1.35	0.282 589	-1.37	0.30	-0.96
04	0.057 814	0.001 343	0.002 117	0.000 049	0.282 619	0.000 010	0.92	1.31	0.282 610	-0.65	0.34	-0.94
05	0.025 764	0.000 359	0.000 898	0.000 013	0.282 599	0.000 008	0.92	1.34	0.282 595	-1.15	0.29	-0.97
06	0.032 659	0.001 029	0.001 168	0.000 036	0.282 602	0.000 012	0.93	1.34	0.282 597	-1.11	0.42	-0.96
07	0.041 359	0.000 428	0.001 356	0.000 014	0.282 614	0.000 011	0.91	1.31	0.282 608	-0.72	0.38	-0.96
08	0.013 921	0.000 543	0.000 432	0.000 015	0.282 579	0.000 009	0.94	1.38	0.282 577	-1.80	0.31	-0.99
09	0.044 354	0.001 332	0.001 426	0.000 042	0.282 612	0.000 009	0.92	1.32	0.282 606	-0.80	0.33	-0.96
10	0.028 804	0.000 658	0.000 975	0.000 024	0.282 610	0.000 008	0.91	1.32	0.282 606	-0.77	0.30	-0.97
11	0.024 080	0.000 362	0.000 795	0.000 010	0.282 604	0.000 010	0.91	1.33	0.282 601	-0.96	0.34	-0.98

Note: $\varepsilon_{Hf}(t)= 10\ 000\times\{[(^{176}Hf/^{177}Hf)_S-(^{176}Lu/^{177}Hf)_S\times(e^{\lambda t}-1)]/[(^{176}Hf/^{177}Hf)_{CHUR,0}-(^{176}Lu/^{177}Hf)_{CHUR}\times(e^{\lambda t}-1)]-1\}$; T_{DM1} is one-stage Hf model age, calculated as $T_{DM1}=1/\lambda\times\ln\{(1+[(^{176}Hf/^{177}Hf)_S-(^{176}Hf/^{177}Hf)_{DM}]/[(^{176}Lu/^{177}Hf)_S-(^{176}Lu/^{177}Hf)_{DM}]\}$; T_{DM2} is two-stage Hf model age, calculated as $T_{DM2}=T_{DM1}-(T_{DM1}-t)\times[(f_{CC}-f_S)/(f_{CC}-f_{DM})]$; where, $\lambda=1.867\times10^{-11}$ yr^{-1} (Söderlund et al., 2004); $(^{176}Lu/^{177}Hf)_S$ and $(^{176}Hf/^{177}Hf)_S$ are the measured values of samples; $(^{176}Lu/^{177}Hf)_{CHUR}=0.033\ 2$ and $(^{176}Hf/^{177}Hf)_{CHUR,0}=0.282\ 772$ (Blichert-Toft and Albarède 1997); $(^{176}Lu/^{177}Hf)_{DM}=0.038\ 4$ and $(^{176}Hf/^{177}Hf)_{DM}=0.283\ 25$ (Griffin et al., 2000); t=crystallization time of zircon.

it will induce concave-upward REE patterns between the middle and heavy REE because of its high partition coefficients for these elements in intermediate to felsic melts (Martin, 2007; Tiepolo et al., 2007). The samples show a progressive decrease in middle and heavy REE with increasing atomic number (Fig. 5a), suggesting breakdown of amphibole during remelting. The breakdown of amphibole plays a key role in dehydration melting, which always supplies initial water to generate melt at the initial stage of melting (Rapp, 1995; Wolf and Wyllie, 1994). In a water-unsaturated source at the lower crust (<8 kbar), an extremely high temperature (thermal gradient >35 ºC/km) would be required for the breakdown of amphibole (Wolf and Wyllie, 1994; Wyllie and Wolf, 1993). Therefore, we infer that the studied graniodiorites were generated through partial melting of a mafic crustal source with normal continental crust thickness at a relatively high thermal gradient (>35 ºC/km).

Most of the studied samples fall on the cotectic lines of the F-An-Or pseudoternary projection (Castro, 2013), which shows that the magma was mainly controlled by the fractionation without any assimilation or mixing (Fig. 6). The minerals that are dominated by the fractional crystallization have been

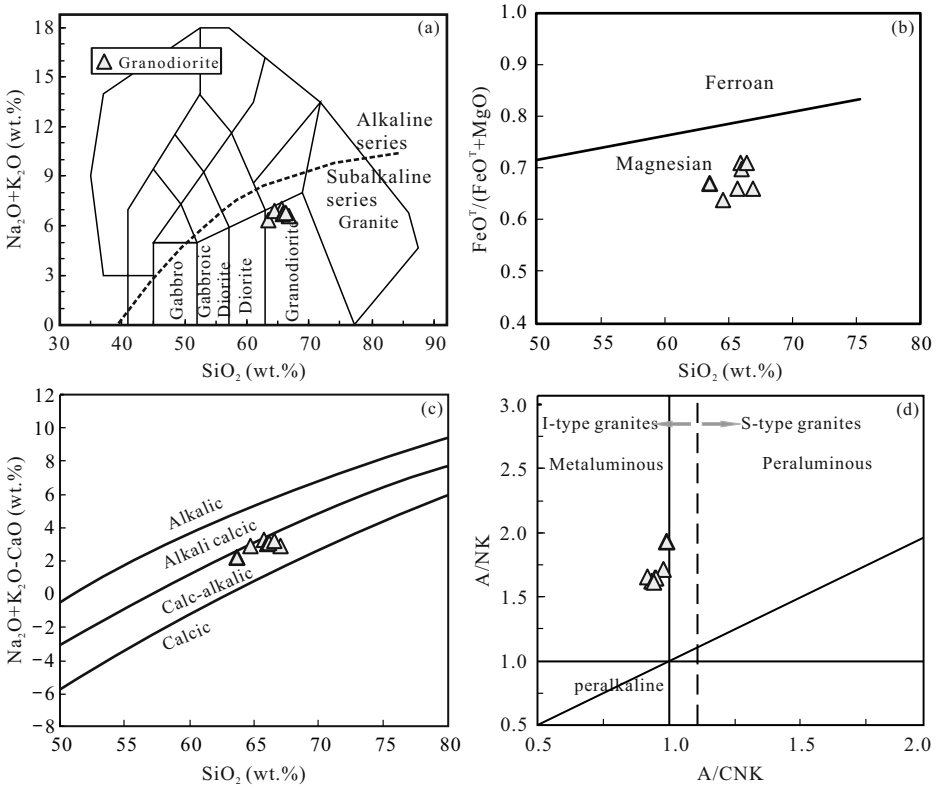

Figure 4. Chemical classifications of the studied granodiorites. (a) Rock classification plots of SiO_2 vs. (Na_2O+K_2O) (Middlemost, 1994); (b) $FeO^T/(FeO^T+MgO)$ vs. SiO_2 diagram (Frost et al., 2001); (c) SiO_2 vs. Na_2O+K_2O-CaO diagram (Frost et al., 2001); (d) A/NK vs. A/CNK diagram (Maniar and Piccoli, 1989; Chappell and White, 1974).

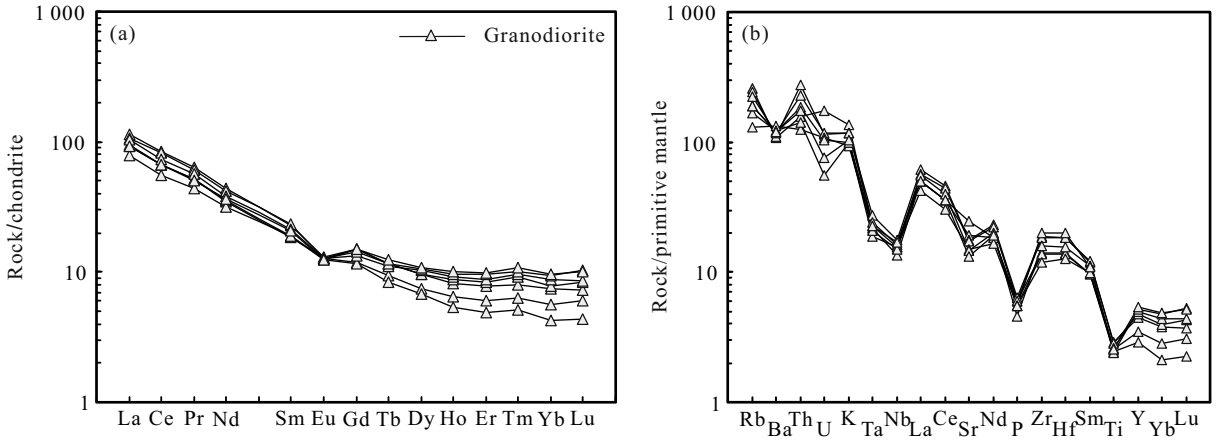

Figure 5. Chondrite-normalized REE patterns and primitive mantle-normalized element spider diagrams for the studied rocks. Chondrite REE abundances are after Taylor and McLennan (1985), trace element abundances for the primitive mantle are after Sun and Mcdonough (1989).

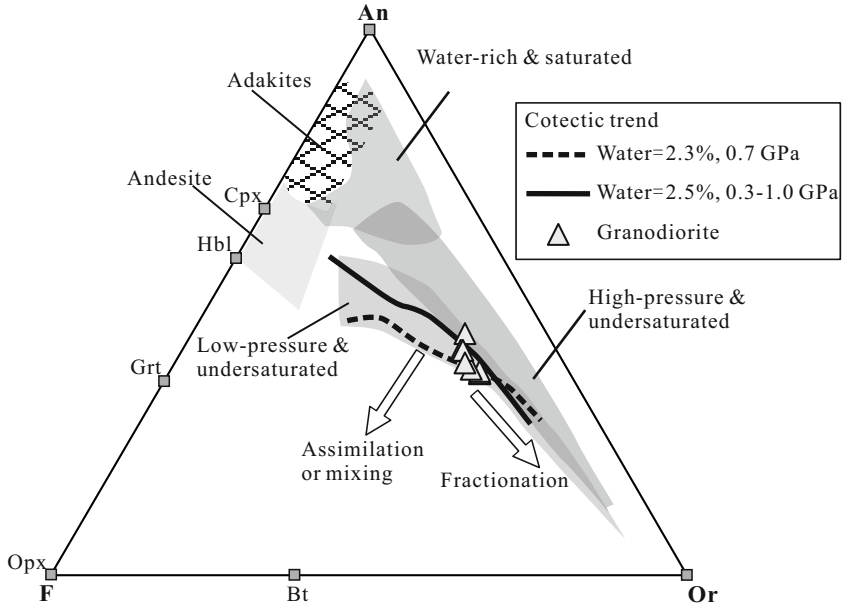

Figure 6. The ternary plot F-An-Or (F=FeO+MgO+MnO; An=anorthite; Or=orthoclase) for the studied granodiorites (Castro, 2013).

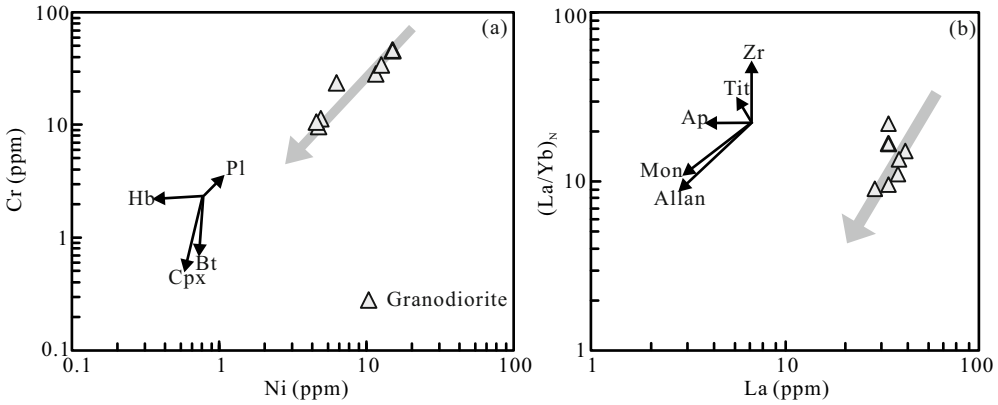

Figure 7. Variations in Cr vs. Ni and $(La/Yb)_N$ vs. La for the studied granodiorites showing the fractional crystallization.

discussed herein. A positive correlation between Cr and Ni strongly suggests biotite and clinopyroxene fractionation (Fig. 7a). Weakly negative Eu anomalies and the correlations between Sr and Eu/Eu* observed in the granodiorites are indicative of small amount of plagioclase fractionation. Accessory minerals are extremely important in controlling the contents of REEs (Gerdes et al., 2009), and the positive correlation between $(La/Yb)_N$ and La suggests that the monazite and allanite are the important fractionated minerals (Fig. 7b).

5.1.2 Source characteristics and its origin

The above discussion has proposed that the felsic melts were generated in lower crust level (LCC), but there are two different types of lower crust in orogenic belts, i.e., ancient basement and juvenile crust. We futher propose that the studied granodioritic melts are partial melts of one juvenile crust, and this juvenile source is the mixing product between mantle- and crust-derived melts during the Paleo-Tethyan subduction. This interpretation is supported by the following evidences.

(1) The zircon U-Pb chronology indicates that the basement rocks (i.e., Xiaomiao Formation) in the EKOB are formed in Paleoproterozoic to Early Mesoproterozoic (1.4–2.5 Ga; Chen et al., 2011; Wang et al., 2004), which is much older than Hf model ages of the studied rocks (~1.3 Ga), as shown in Fig. 9. Such differences imply that the source contains a certain amount of crustal materials younger than the basement.

(2) The studied granodiorites are isotopically more depleted than the ancient basement with higher $\varepsilon_{Hf}(t)$ values (-1.80 to -0.65), displaying overlapping Lu-Hf isotopic compositions with the mantle-derived gabbroic rocks (Fig. 9) (Xiong et al., 2014; Chen et al., 2007a), which suggests that the magma source was closely related to the mantle material, either by the direct input of mantle-derived mafic melts or by remelting of a juvenile mantle-derived mafic lower crust.

No mafic or quartz diorite enclaves were found in the granodiorite, precluding an origin of magma mixing between mafic and felsic magmas (Xia et al., 2014; Xiong et al., 2014; Barbarin and Didier, 1992), which is consistent with the diagram of F-An-Or (Fig. 6). Thus, since the possibility of fractional crystallization of basaltic magma has been ruled out, we attribute their mantle imprintings to juvenile mafic lower crust.

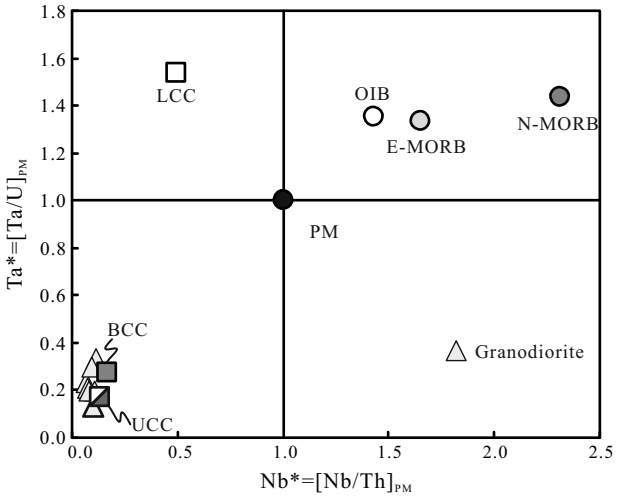

Figure 8. Diagram of Ta* vs. Nb* for the studied granodiorites (after Niu and Batiza, 1997). Data of primitive mantle and average oceanic basalts (OIB, E-MORB, N-MORB) are from Sun and McDonough (1989). Crust compositions (BCC, LCC, UCC) are from Rudnick and Gao (2003).

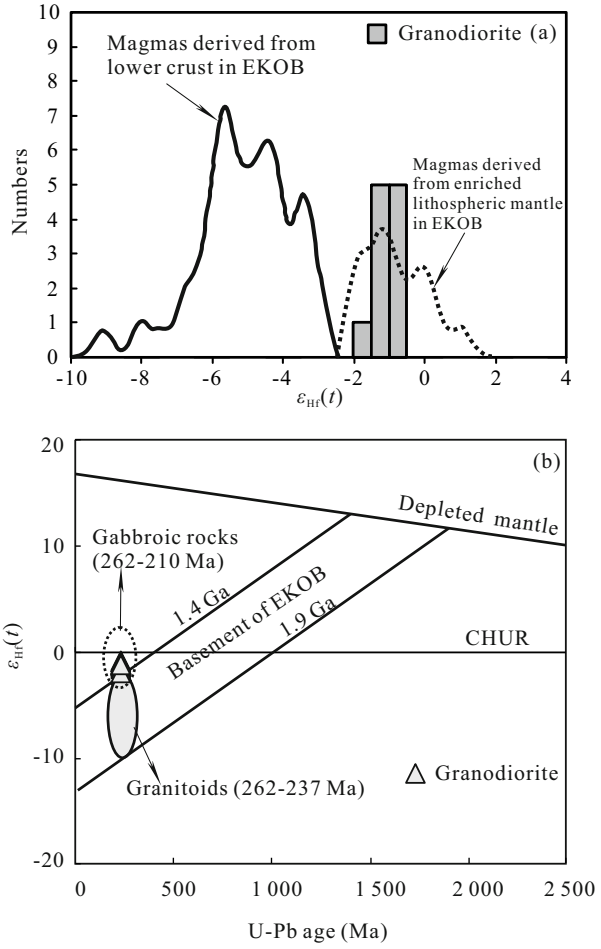

Figure 9. (a) Histogram of $\varepsilon_{Hf}(t)$ and (b) plots of $\varepsilon_{Hf}(t)$ vs. U-Pb ages for zircons from studied granodiorites (the values used for constructing the depleted mantle and crust reference evolution lines are after Griffin et al. (2002, 2000). Data of lower crust and enriched lithospheric mantle are from Chen et al. (2014), Ding et al. (2014), Xiong et al. (2014, 2013, 2012, 2011b).

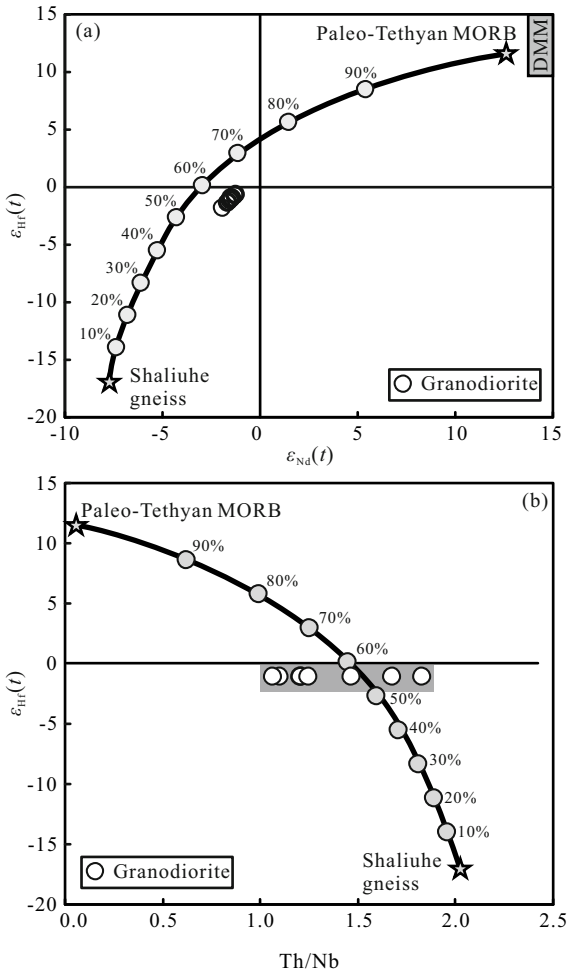

Figure 10. Isotopic modeling showing the studied granodiorites plot along an apparent 'mixing' trend between Paleo-Tethyan MORB and terrestrial sediments (Shaliuhe gneiss).

The juvenile materials were formed by crust-mantle interaction, as evidenced by the ratios of incompatible elements and Hf isotopes of the studied rocks. Incompatible element ratios are strictly controlled by the source, which is not influenced by the processes of fractional crystallization and partial melting (Hu et al., 2015; Pearce and Norry, 1979). The studied felsic rocks show average ratios of Zr/Y (9.12) and Sm/Nd (0.18) resemble the the upper crust (UCC) (Zr/Y=9.19, Sm/Nd=0.17 [UCC] vs. Zr/Y=4.25, Sm/Nd=0.26 [LCC]) (Rudnick and Gao, 2003). In the diagram of Ta* vs. Nb* (Fig. 8), the granodiorites show also closely ratios resemble the UCC, which suggests the upper crustal materials have significant contribution to the generation of the juvenile lower crust.

The supracrustal signature of incompatible element ratios and the enriched mantle signature of Hf isotopes might reflect the juvenile lower crust was formed by a hybrid source consisting of the lithospheric mantle and ancient supracrustal crust. The addition of the ancient supracrustal materials will lead to the juvenile lower crust has old modal age (~1.3 Ga).

Owing to the intensive basaltic magma underplating and crust-mantle interaction during the Late Permian–Early Triassic (Liu et al., 2014; Xiong et al., 2013, 2012), one juvenile lower crust formed by magma mixing lithospheric mantle and supra-

crustal melts (Ding et al., 2014; Xiong et al., 2012; Zhang et al., 2012). Partial melting of such juvenile lower crust would produce felsic melts parental to the studied granodiorites in the EKOB. We attempt to estimate the relative proportions of crust and mantle contributions to the juvenile lower crust in terms of trace elements and isotopes (Fig. 10). We choose two end members: (1) MORB-like basalts from the Buqingshan Paleo-Tethyan ophiolite as representing the contemporary Paleo-Tethyan mantle component (Bian et al., 2004); (2) Shaliuhe gneiss forming the major component of the supracrustal rocks in the EKOB as representing the crustal component (Chen et al., 2007b; Harris et al., 1988). Our modeling calculation shows that at least 40%–45% supracrustal materials contributed to the mantle-derived mafic melts (Fig. 10).

5.2 Geological Implications

The low pressure environment of the felsic melt (0.7–1 GPa; Fig. 6) indicates that the magma was derived from lower crust with normal crustal thickness. Thus, according to the normal temperature gradient (~25 ºC/km), the temperature will not exceed 750 ºC, which is much lower than the apatite saturation temperature of the studied pluton (1 123–1 163 ºC; calculated by the formula of Harrison and Watson, 1984). Therefore, the external high temperature heat source is required, and this conclusion is consistent with the above discussion, i.e., the studied high-K calc-alkaline granitoid rocks (~234 Ma) were probably derived from partial melting of juvenile lower crust at a high thermal gradient (>35 ºC/km).

High temperature gradient in normal continental crust level is most likely to occur in the post-collisional extension setting. During the extension of the lithosphere, basaltic magma underplating would cause significant temperature elevation at the lower crustal level. The joint effect of heating and decompression may have triggered partial melting of the lower crust in the EKOB. Thus, melting of the juvenile lower crust in the EKOB is mainly attributed to the post-collisional extension.

The proposal of post-collisional extension is consistent with the type and characteristics of the Late Paleozoic–Early Mesozoic magmatism in the EKOB. As shown in Fig. 11, the

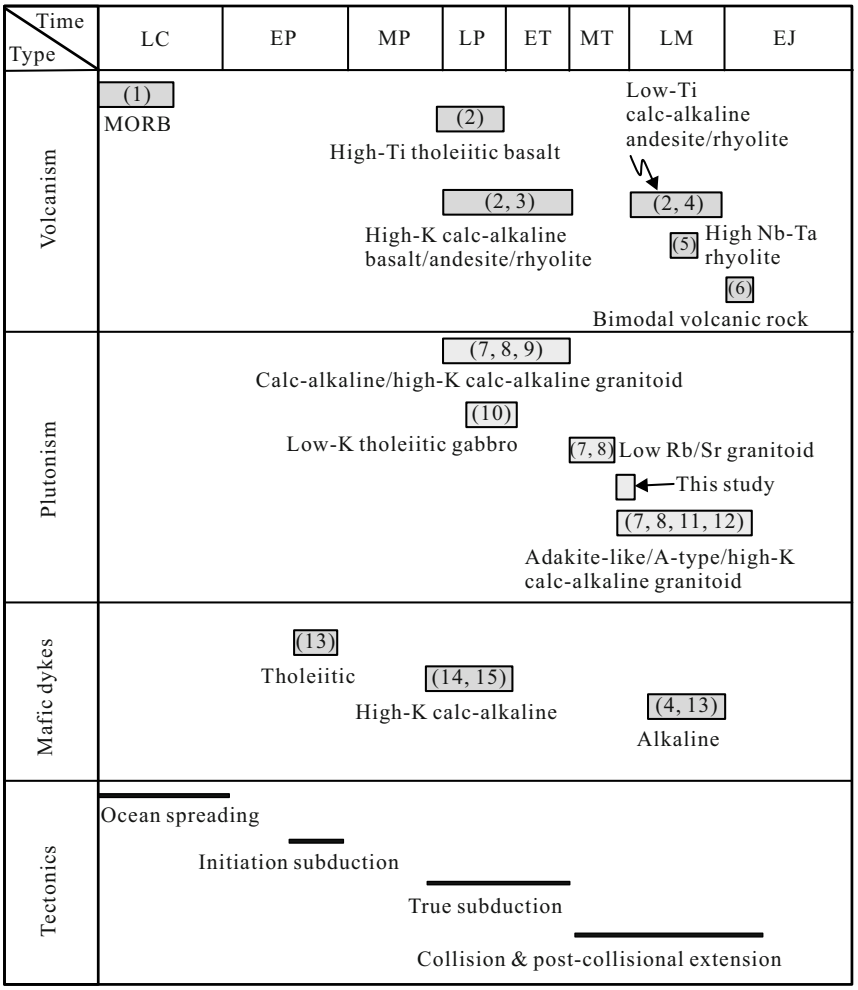

Figure 11. The diagram of magma-tectonic evolution cycle showing the volcanism, plutonism and mafic dykes during the Paleo-Tethyan orogeny in the East Kunlun. E-early, M-middle, L-late, C-Carboniferous, P-Permian, T-Triassic, J-Jurassic. Relevant references are listed as following: (1) Yang et al. (2009), (2) Yang et al. (2005), (3) Li et al. (2015), (4) Hu et al. (2015), (5) Ding et al. (2011), (6) Zhu et al. (2003), (7) Xiong et al. (2014), (8) Zhang et al. (2012), (9) Xiong et al. (2011a), (10) Chen et al. (2012), (11) Xia et al. (2014), (12) Yuan et al. (2009), (13) Ma et al. (2012), (14) Xiong et al. (2013), (15) Xiong et al. (2011b).

Late Carboniferous MORB in the A'nyemaqen suture zone marks the spreading of the Paleo-Tethyan Ocean (Yang et al., 2009), the Early Permian tholeiitic mafic dyke swarms suggests the initial subduction of the ocean basin (Liu et al., 2014), and the Late Permian to Early Triassic large scale calc-alkaline magmatism constitutes the giant magma arc in the EKOB (Li et al., 2015; Xiong et al., 2014, 2012). More importantly, large amount of extension-related magmatism occured since the late stage of Middle Triassic, such as the alkaline mafic dyke swarm, A-type granitoids, adakite-like granitoids, high Nb-Ta rhyolites and the bimodal volcanic rocks (Hu et al., 2015; Xia et al., 2014; Xiong et al., 2014; Ding et al., 2011; Zhu et al., 2003), which indicates that the post-collisional extension could occur as early as 235 Ma in the EKOB.

This study shows the relationship between the origin of high-K calc-alkaline granodiorite, and the growth and evolution of continental crust through magmatism during orogeny. For a long time, there is a general consensus about the contribution of high-K calc-alkaline granodioritic batholiths to the growth and evolution of the continent crust since Late Archean (Condie, 2014; Hawkesworth et al., 2010). This study proposes that high-K calc-alkaline granodiorities could be derived from melting of the juvenile lower crustal during post-collisional extension, but the juvenile source was formed earlier by crust-mantle interaction during the slab subduction.

6 CONCLUSIONS

Based on zircon U-Pb dating and Hf isotopic analysis, as well as whole-rock geochemical analysis of the granodiorites in the eastern section of EKOB, the following conclusions can be drawn.

(1) The studied granodiorites yield zircon U-Pb ages of 235 Ma, and their geochemical compositions show that they are typical high-K calc-alkaline, magnesian, metaluminous I-type granitoids.

(2) The granodiorites exhibit enrichment of LREE with flat HREE patterns [$(Gd/Yb)_N$=1.52–2.73], coupled with high Mg# (42–50) and high $\varepsilon_{Hf}(t)$ values from -0.65 to -1.80, indicating that they were derived from partial melting of a juvenile mafic crustal source within normal crust thickness.

(3) The supracrustal signature of incompatible element ratios and the enriched mantle signature of Hf isotopes might reflect the juvenile lower crust was formed by mixing between lithospheric mantle-derived melt and supracrustal melt (40%–45%) during the seafloor subduction.

(4) The petrogenesis of Middle Triassic granitoids in the EKOB was probably related to the post-collisional extension that caused the basaltic magma underplating, which triggered partial melting of the juvenile lower crust.

ACKNOWLEDGMENTS

The authors are grateful to the anonymous reviewers and editors for their constructive comments to improve the paper. This study was financially supported by the China Geological Survey (Nos. 12120115069701, 12120113095700 and 1212011220391), the National Natural Science Foundation of China (No. 41272079), the China Postdoctoral Science Foundation-China (No. 2015M582529), the State Key Laboratory of Continental Tectonics and Dynamics (No. K201508) and the Special Financial Support Program of Central Government for Local Universities (No. 80000-14Z019). The final publication is available at Springer via http://dx.doi.org/10.1007/s12583-016-0674-6.

REFERENCES CITED

Ajaji, T., Weis, D., Giret, A., et al., 1998. Coeval Potassic and Sodic Calc-Alkaline Series in the Post-Collisional Hercynian Tanncherfi Intrusive Complex, Northeastern Morocco: Geochemical, Isotopic and Geochronological Evidence. *Lithos*, 45(1–4): 371–393. doi:10.1016/s0024-4937(98)00040-1

Barbarin, B., Didier, J., 1992. Genesis and Evolution of Mafic Microgranular Enclaves through Various Types of Interaction between Coexisting Felsic and Mafic Magmas. *Transactions of the Royal Society of Edinburgh*: *Earth Sciences*, 83(1/2): 145–153. doi:10.1017/s0263593300007835

Beard, J. S., Lofgren, G. E., 1991. Dehydration Melting and Water-Saturated Melting of Basaltic and Andesitic Greenstones and Amphibolites at 1, 3, and 6.9 kb. *Journal of Petrology*, 32(2): 365–401. doi:10.1093/petrology/32.2.365

Beard, J., Ragland, P., Rushmer, T., 2004. Hydration Crystallization Reactions between Anhydrous Minerals and Hydrous Melt to Yield Amphibole and Biotite in Igneous Rocks: Description and Implications. *The Journal of Geology*, 112(5): 617–621. doi:10.1086/422670

Bellos, L. I., Castro, A., Díaz-Alvarado, J., et al., 2015. Multi-Pulse Cotectic Evolution and In-Situ Fractionation of Calc-Alkaline Tonalite-granodiorite Rocks, Sierra de Velasco Batholith, Famatinian Belt, Argentina. *Gondwana Research*, 27(1): 258–280. doi:10.1016/j.gr.2013.09.019

Bergemann, C., Jung, S., Berndt, J., et al., 2014. Generation of Magnesian, High-K Alkali-Calcic Granites and Granodiorites from Amphibolitic Continental Crust in the Damara Orogen, Namibia. *Lithos*, 198/199: 217–233. doi:10.1016/j.lithos.2014.03.033

Bian, Q. T., Li, D. H., Pospelov, I., et al., 2004. Age, Geochemistry and Tectonic Setting of Buqingshan Ophiolites, North Qinghai-Tibet Plateau, China. *Journal of Asian Earth Sciences*, 23(4): 577–596. doi:10.1016/j.jseaes.2003.09.003

Blichert-Toft, J., Albarède, F., 1997. The Lu-Hf Isotope Geochemistry of Chondrites and the Evolution of the Mantle-Crust System. *Earth and Planetary Science Letters*, 148(1/2): 243–258

Bouilhol, P., Jagoutz, O., Hanchar, J. M., et al., 2013. Dating the India-Eurasia Collision through Arc Magmatic Records. *Earth and Planetary Science Letters*, 366: 163–175. doi:10.1016/j.epsl.2013.01.023

Bucholz, C. E., Jagoutz, O., Schmidt, M. W., et al., 2014. Fractional Crystallization of High-K Arc Magmas: Biotite-Versus Amphibole-Dominated Fractionation Series in the Dariv Igneous Complex, Western Mongolia. *Contributions to Mineralogy and Petrology*, 168(5): 1–28. doi:10.1007/s00410-014-1072-9

Castro, A., 2013. Tonalite-Granodiorite Suites as Cotectic Sys-

tems: A Review of Experimental Studies with Applications to Granitoid Petrogenesis. *Earth-Science Reviews*, 124: 68–95. doi:10.1016/j.earscirev.2013.05.006

Castro, A., 2014. The Off-Crust Origin of Granite Batholiths. *Geoscience Frontiers*, 5(1): 63–75. doi:10.1016/j.gsf.2013.06.006

Chappell, B. W., 1999. Aluminium Saturation in I- and S-Type Granites and the Characterization of Fractionated Haplogranites. *Lithos*, 46(3): 535–551. doi:10.1016/s0024-4937(98)00086-3

Chappell, B. W., White, A. J. R., 1974. Two Contrasting Granite Types. *Pacific Geology*, 8: 173–174

Chappell, B. W., White, A. J. R., 2001. Two Contrasting Granite Types: 25 Years Later. *Australian Journal of Earth Sciences*, 48(4): 489–499. doi:10.1046/j.1440-0952.2001.00882.x

Chen, N. S., Wang, X. Y., Zhang, H. F., et al., 2007a. Geochemistry and Nd-Sr-Pb Isotopic Compositions of Granitoids from Qaidam and Oulongbuluke Micro-Blocks, NW China: Constraints on Basement Nature and Tectonic Affinity. *Earth Science—Jorunal of China University of Geosciences*, 32(1): 7–21 (in Chinese with English Abstract)

Chen, N. S., Xia, X. P., Li, X. Y., et al., 2007b. Timing of Magmatism of the Gneissic-Granite Plutons along North Qaidam Margin and Implications for Precambrian Crustal Accretions: Zircon U-Pb Dating and Hf Isotope Evidences. *Acta Petrologica Sinica*, 23(2): 501–512 (in Chinese with English Abstract)

Chen, X. H., Gehrels, G., Yin, A., et al., 2012. Paleozoic and Mesozoic Basement Magmatisms of Eastern Qaidam Basin, Northern Qinghai-Tibet Plateau: LA-ICP-MS Zircon U-Pb Geochronology and Its Geological Significance. *Acta Geologica Sinica—English Edition*, 86(2): 350–369. doi:10.1111/j.1755-6724.2012.00665.x

Chen, X. H., Gehrels, G., Yin, A., et al., 2015. Geochemical and Nd-Sr-Pb-O Isotopic Constrains on Permo-Triassic Magmatism in Eastern Qaidam Basin, Northern Qinghai-Tibetan Plateau: Implications for the Evolution of the Paleo-Tethys. *Journal of Asian Earth Sciences*, 114: 674–692. doi:10.1016/j.jseaes.2014.11.013

Chen, Y. X., Pei, X. Z., Li, R. B., et al., 2011. Zircon U-Pb Age of Xiaomiao Formation of Proterozoic in the Eastern Section of the East Kunlun Orogenic Belt. *Geoscience*, 25(3): 510–521 (in Chinese with English Abstract)

Cocherie, A., Rossi, P., Fouillac, A. M., et al., 1994. Crust and Mantle Contributions to Granite Genesis—An Example from the Variscan Batholith of Corsica, France, Studied by Trace-Element and Nd-Sr-O Isotope Systematics. *Chemical Geology*, 115(3/4): 173–211. doi:10.1016/0009-2541(94)90186-4

Condie, K. C., 2014. Growth of Continental Crust: A Balance between Preservation and Recycling. *Mineralogical Magazine*, 78(3): 623–637. doi:10.1180/minmag.2014.078.3.11

Corfu, F., 2003. Atlas of Zircon Textures. *Reviews in Mineralogy and Geochemistry*, 53(1): 469–500. doi:10.2113/0530469

DePaolo, D. J., 1981. Trace Element and Isotopic Effects of Combined Wallrock Assimilation and Fractional Crystallization. *Earth and Planetary Science Letters*, 53(2): 189–202. doi:10.1016/0012-821x(81)90153-9

Ding, Q. F., Jiang, S. Y., Sun, F. Y., 2014. Zircon U-Pb Geochronology, Geochemical and Sr-Nd-Hf Isotopic Compositions of the Triassic Granite and Diorite Dikes from the Wulonggou Mining Area in the Eastern Kunlun Orogen, NW China: Petrogenesis and Tectonic Implications. *Lithos*, 205: 266–283. doi:10.1016/j.lithos.2014.07.015

Ding, S., Huang, H., Niu, Y. L., et al., 2011. Geochemistry, Geochronology and Petrogenesis of East Kunlun High Nb-Ta Rhyolites. *Acta Petrologica Sinica*, 27: 3603–3614 (in Chinese with English Abstract)

Eyal, M., Litvinovsky, B., Jahn, B. M., et al., 2010. Origin and Evolution of Post-Collisional Magmatism: Coeval Neoproterozoic Calc-Alkaline and Alkaline Suites of the Sinai Peninsula. *Chemical Geology*, 269(3/4): 153–179. doi:10.1016/j.chemgeo.2009.09.010

Frost, B. R., 2001. A Geochemical Classification for Granitic Rocks. *Journal of Petrology*, 42(11): 2033–2048. doi:10.1093/petrology/42.11.2033

Gerdes, A., Kemp, A. I. S., Hanchar, J. M., et al., 2009. Accessory Minerals as Tracers of Crustal Processes. *Chemical Geology*, 261(3/4): 197–198. doi:10.1016/j.chemgeo.2009.03.001

Gong, S. L., Chen, N. S., Geng, H. Y., et al., 2014. Zircon Hf Isotopes and Geochemistry of the Early Paleoproterozoic High-Sr Low-Y Quartz-Diorite in the Quanji Massif, NW China: Crustal Growth and Tectonic Implications. *Journal of Earth Science*, 25(1): 74–86. doi:10.1007/s12583-014-0401-2

Griffin, W. L., Pearson, N. J., Belousova, E., et al., 2000. The Hf Isotope Composition of Cratonic Mantle: LAM-MC-ICPMS Analysis of Zircon Megacrysts in Kimberlites. *Geochimica et Cosmochimica Acta*, 64(1): 133–147. doi:10.1016/s0016-7037(99)00343-9

Griffin, W. L., Wang, X., Jackson, S. E., et al., 2002. Zircon Chemistry and Magma Mixing, SE China: In-Situ Analysis of Hf Isotopes, Tonglu and Pingtan Igneous Complexes. *Lithos*, 61(3/4): 237–269. doi:10.1016/s0024-4937(02)00082-8

Harris, N. B. W., Xu, R. H., Lewis, C. L., et al., 1988. Isotope Geochemistry of the 1985 Tibet Geotraverse, Lhasa to Golmud. *Philosophical Transactions of the Royal Society A*: *Mathematical*, *Physical and Engineering Sciences*, 327(1594): 263–285. doi:10.1098/rsta.1988.0129

Harrison, T. M., Watson, E. B., 1984. The Behavior of Apatite during Crustal Anatexis: Equilibrium and Kinetic Considerations. *Geochimica et Cosmochimica Acta*, 48(7): 1467–1477. doi:10.1016/0016-7037(84)90403-4

Hawkesworth, C. J., Dhuime, B., Pietranik, A. B., et al., 2010. The Generation and Evolution of the Continental Crust. *Journal of the Geological Society*, 167(2): 229–248. doi:10.1144/0016-76492009-072

Honarmand, M., Omran, N. R., Neubauer, F., et al., 2015. Geochemistry of Enclaves and Host Granitoids from the Kashan Granitoid Complex, Central Iran: Implications for

Enclave Generation by Interaction of Cogenetic Magmas. *Journal of Earth Science*, 26(5): 626–647. doi:10.1007/s12583-015-0584-1

Hoskin, P. W. O., Schaltegger, U., 2003. The Composition of Zircon and Igneous and Metamorphic Petrogenesis. *Reviews in Mineralogy and Geochemistry*, 53(1): 27–62. doi:10.2113/0530027

Hu, Y., Niu, Y. L., Li, J. Y., et al., 2015. Petrogenesis and Tectonic Significance of the Late Triassic Mafic Dikes and Felsic Volcanic Rocks in the East Kunlun Orogenic Belt, Northern Tibet Plateau. *Lithos*, 245(2): 205–222. doi:10.1016/j.lithos.2015.05.004

Hu, Z. C., Liu, Y. S., Gao, S., et al., 2012. Improved in Situ Hf Isotope Ratio Analysis of Zircon Using Newly Designed X Skimmer Cone and Jet Sample Cone in Combination with the Addition of Nitrogen by Laser Ablation Multiple Collector ICP-MS. *Journal of Analytical Atomic Spectrometry*, 27: 1391–1399. doi:10.1039/c2ja30078h

Jagoutz, O., Schmidt, M. W., Enggist, A., et al., 2013. TTG-Type Plutonic Rocks Formed in a Modern Arc Batholith by Hydrous Fractionation in the Lower Arc Crust. *Contributions to Mineralogy and Petrology*, 166(4): 1099–1118. doi:10.1007/s00410-013-0911-4

Jung, S., Masberg, P., Mihm, D., et al., 2009. Partial Melting of Diverse Crustal Sources—Constraints from Sr-Nd-O Isotope Compositions of Quartz Diorite-granodiorite-leucogranite Associations (Kaoko Belt, Namibia). *Lithos*, 111(3/4): 236–251. doi:10.1016/j.lithos.2008.10.010

Li, X., Huang, X., Luo, M., et al., 2015. Petrogenesis and Geodynamic Implications of the Mid-Triassic Lavas from East Kunlun, Northern Tibetan Plateau. *Journal of Asian Earth Sciences*, 105: 32–47. doi:10.1016/j.jseaes.2015.03.009

Liu, B., Ma, C. Q., Zhang, J., et al., 2014. ^{40}Ar-^{39}Ar Age and Geochemistry of Subduction-Related Mafic Dikes in Northern Tibet, China: Petrogenesis and Tectonic Implications. *International Geology Review*, 56(1): 57–73. doi:10.1080/00206814.2013.818804

Liu, Y. S., Gao, S., Hu, Z. C., et al., 2010. Continental and Oceanic Crust Recycling-Induced Melt-Peridotite Interactions in the Trans-North China Orogen: U-Pb Dating, Hf Isotopes and Trace Elements in Zircons from Mantle Xenoliths. *Journal of Petrology*, 51(1/2): 537–571. doi:10.1093/petrology/egp082

Ludwig, K. R., 2003. User's Manual for Isoplot/Ex Version 3.00: A Geochronological Toolkit for Microsoft Excel. Berkeley Geochronology Center, Special Publication

Ma, C. Q., Zhang, J. Y., Xiong, F. H., et al., 2012. Mantle Evolution from Plate Subduction to Post-Orogenic Extension: Evidence from Permo-Triassic Mafic Dike Swarms in Northern Tibet Plateau. *Mineralogical Magazine*, 76: 2046

Maniar, P. D., Piccoli, P. M., 1989. Tectonic Discrimination of Granitoids. *Geological Society of America Bulletin*, 101(5): 635–643. doi:10.1130/0016-7606(1989)101<0635:tdog>2.3.co;2

Martin, R. F., 2007. Amphiboles in the Igneous Environment. *Reviews in Mineralogy and Geochemistry*, 67(1): 323–358. doi:10.2138/rmg.2007.67.9

Middlemost, E. A. K., 1994. Naming Materials in the Magma/Igneous Rock System. *Earth-Science Reviews*, 37(3/4): 215–224. doi:10.1016/0012-8252(94)90029-9

Mo, X. X., Dong, G. C., Zhao, Z. D., et al., 2009. Mantle Input to the Crust in Southern Gangdese, Tibet, during the Cenozoic: Zircon Hf Isotopic Evidence. *Journal of Earth Science*, 20(2): 241–249. doi:10.1007/s12583-009-0023-2

Niu, Y. L., Batiza, R., 1997. Trace Element Evidence from Seamounts for Recycled Oceanic Crust in the Eastern Pacific Mantle. *Earth and Planetary Science Letters*, 148(3/4): 471–483. doi:10.1016/s0012-821x(97)00048-4

Ostendorf, J., Jung, S., Berndt-Gerdes, J., et al., 2014. Syn-Orogenic High-Temperature Crustal Melting: Geochronological and Nd-Sr-Pb Isotope Constraints from Basement-Derived Granites (Central Damara Orogen, Namibia). *Lithos*, 192–195: 21–38. doi:10.1016/j.lithos.2014.01.007

Pearce, J. A., Norry, M. J., 1979. Petrogenetic Implications of Ti, Zr, Y, and Nb Variations in Volcanic Rocks. *Contributions to Mineralogy and Petrology*, 69(1): 33–47. doi:10.1007/bf00375192

Pitcher, W. S., 1987. Granites and yet more Granites Forty Years on. *Geologische Rundschau*, 76(1): 51–79. doi:10.1007/bf01820573

Rapp, R. P., 1995. Amphibole-out Phase Boundary in Partially Melted Metabasalt, Its Control over Liquid Fraction and Composition, and Source Permeability. *Journal of Geophysical Research*, 100(B8): 15601–15610. doi:10.1029/95jb00913

Rapp, R. P., Watson, E. B., 1995. Dehydration Melting of Metabasalt at 8–32 kbar: Implications for Continental Growth and Crust-Mantle Recycling. *Journal of Petrology*, 36(4): 891–931. doi:10.1093/petrology/36.4.891

Rapp, R. P., Watson, E. B., Miller, C. F., 1991. Partial Melting of Amphibolite/Eclogite and the Origin of Archean Trondhjemites and Tonalites. *Precambrian Research*, 51(1–4): 1–25. doi:10.1016/0301-9268(91)90092-o

Roger, F., Arnaud, N., Gilder, S., et al., 2003. Geochronological and Geochemical Constraints on Mesozoic Suturing in East Central Tibet. *Tectonics*, 22(4): 1037. doi:10.1029/2002tc001466

Rudnick, R. L., Gao, S., 2003. Composition of the Continental Crust. *Treatise on Geochemistry*, 33: 1–64. doi:10.1016/b0-08-043751-6/03016-4

Simon, J. I., Weis, D., DePaolo, D. J., et al., 2014. Assimilation of Preexisting Pleistocene Intrusions at Long Valley by Periodic Magma Recharge Accelerates Rhyolite Generation: Rethinking the Remelting Model. *Contributions to Mineralogy and Petrology*, 167(1): 1–34. doi:10.1007/s00410-013-0955-5

Sisson, T. W., Ratajeski, K., Hankins, W. B., et al., 2004. Voluminous Granitic Magmas from Common Basaltic Sources. *Contributions to Mineralogy and Petrology*, 148(6): 635–661. doi:10.1007/s00410-004-0632-9

Söderlund, U., Patchett, P. J., Vervoort, J. D., et al., 2004. The ^{176}Lu Decay Constant Determined by Lu-Hf and U-Pb Isotope Systematics of Precambrian Mafic Intrusions.

Earth and Planetary Science Letters, 219(3/4): 311–324.

Soesoo, A., 2000. Fractional Crystallization of Mantle-Derived Melts as a Mechanism for some I-Type Granite Petrogenesis: An Example from Lachlan Fold Belt, Australia. *Journal of the Geological Society*, *London*, 157(1): 135–149. doi:10.1144/jgs.157.1.135

Sun, S. S., McDonough, W. F., 1989. Chemical and Isotopic Systematics of Oceanic Basalts: Implications for Mantle Composition and Processes. *Geological Society*, *London*, *Special Publications*, 42(1): 313–345. doi:10.1144/gsl.sp.1989.042.01.19

Taylor, S. R., McLennan, S. M., 1985. The Continental Crust: Its Composition and Evolution. Blackwell Scientific Publications, Oxford

Tiepolo, M., Oberti, R., Zanetti, A., et al., 2007. Trace-Element Partitioning between Amphibole and Silicate Melt. *Reviews in Mineralogy and Geochemistry*, 67(1): 417–452. doi:10.2138/rmg.2007.67.11

Wang, G. C., Wang, Q. H., Jian, P., et al., 2004. Zircon SHRIMP Ages of Precambrian Metamorphic Basement Rocks and Their Tectonic Significance in the Eastern Kunlun Mountains, Qinghai Province, China. *Earth Science Frontiers*, 11(4): 481–490 (in Chinese with English Abstract)

Wolf, M. B., Wyllie, P. J., 1994. Dehydration-Melting of Amphibolite at 10 kbar: The Effects of Temperature and Time. *Contributions to Mineralogy and Petrology*, 115(4): 369–383. doi:10.1007/bf00320972

Wyllie, P. J., Wolf, M. B., 1993. Amphibolite Dehydration-Melting: Sorting out the Solidus. *Geological Society*, *London*, *Special Publications*, 76(1): 405–416. doi:10.1144/gsl.sp.1993.076.01.20

Xia, R., Wang, C. M., Deng, J., et al., 2014. Crustal Thickening Prior to 220 Ma in the East Kunlun Orogenic Belt: Insights from the Late Triassic Granitoids in the Xiao-Nuomuhong Pluton. *Journal of Asian Earth Sciences*, 93: 193–210. doi:10.1016/j.jseaes.2014.07.013

Xiong, F. H., Ma, C. Q., Jiang, H. A., et al., 2013. Petrogenetic and Tectonic Significance of Permian Calc-Alkaline Lamprophyres, East Kunlun Orogenic Belt, Northern Qinghai-Tibet Plateau. *International Geology Review*, 55(14): 1817–1834. doi:10.1080/00206814.2013.804683

Xiong, F. H., Ma, C. Q., Zhang, J. Y., et al., 2011a. Zircon LA-ICP-MS U-Pb Dating and Geological Significance of Bairiqili Gabbro Pluton in Eastern Kunlun, Northern Qinghai-Tibet Plateau. *Geological Bulletin of China*, 30(8): 1196–1202 (in Chinese with English Abstract)

Xiong, F. H., Ma, C. Q., Zhang, J. Y., et al., 2011b. LA-ICP-MS Zircon U-Pb Dating, Elements and Sr-Nd-Hf Isotope Geochemistry of the Early Mesozoic Mafic Dyke Swarms in Eastern Kunlun Orogenic Belt. *Acta Petrologica Sinica*, 27: 3350–3364 (in Chinese with English Abstract)

Xiong, F. H., Ma, C. Q., Zhang, J. Y., et al., 2012. The Origin of Mafic Microgranular Enclaves and Their Host Granodiorites from East Kunlun, Northern Qinghai-Tibet Plateau: Implications for Magma Mixing during Subduction of Paleo-Tethyan Lithosphere. *Mineralogy and Petrology*, 104(3/4): 211–224. doi:10.1007/s00710-011-0187-1

Xiong, F. H., Ma, C. Q., Zhang, J. Y., et al., 2014. Reworking of Old Continental Lithosphere: An Important Crustal Evolution Mechanism in Orogenic Belts, as Evidenced by Triassic I-Type Granitoids in the East Kunlun Orogen, Northern Tibetan Plateau. *Journal of the Geological Society*, 171(6): 847–863. doi:10.1144/jgs2013-038

Xu, M. J., Li, C., Xu, W., et al., 2014. Petrology, Geochemistry and Geochronology of Gabbros from the Zhongcang Ophiolitic Mélange, Central Tibet: Implications for an Intra-Oceanic Subduction Zone within the Neo-Tethys Ocean. *Journal of Earth Science*, 25(2): 224–240. doi:10.1007/s12583-014-0419-5

Xu, Z. Q., Yang, J. S., Jiang, M., et al., 2001. Deep Structure and Lithospheric Shear Faults in the East Kunlun-Qiangtang Region, Northern Tibetan Plateau. *Science in China Series D*: *Earth Sciences*, 44(S1): 1–9. doi:10.1007/bf02911965

Yang, J. S., Robinson, P. T., Jiang, C. F., et al., 1996. Ophiolites of the Kunlun Mountains, China and Their Tectonic Implications. *Tectonophysics*, 258(1–4): 215–231. doi:10.1016/0040-1951(95)00199-9

Yang, J. S., Shi, R. D., Wu, C. L., et al., 2009. Dur'ngoi Ophiolite in East Kunlun, Northeast Tibetan Plateau: Evidence for Paleo-Tethyan Suture in Northwest China. *Journal of Earth Science*, 20(2): 303–331. doi:10.1007/s12583-009-0027-y

Yang, J. S., Xu, Z. Q., Li, H. B., et al., 2005. The Paleo-Tethyan Volcanism and Plate Tectonic Regime in the A'nyemaqen Region of East Kunlun, Northern Tibet Plateau. *Acta Petrologica et Mineralogica*, 24(5): 369–380 (in Chinese with English Abstract)

Yuan, C., Sun, M., Xiao, W. J., et al., 2009. Garnet-Bearing Tonalitic Porphyry from East Kunlun, Northeast Tibetan Plateau: Implications for Adakite and Magmas from the MASH Zone. *International Journal of Earth Sciences*, 98(6): 1489–1510. doi:10.1007/s00531-008-0335-y

Zhang, J. Y., Ma, C. Q., Xiong, F. H., et al., 2012. Petrogenesis and Tectonic Significance of the Late Permian–Middle Triassic Calc-Alkaline Granites in the Balong Region, Eastern Kunlun Orogen, China. *Geological Magazine*, 149(5): 892–908. doi:10.1017/s0016756811001142

Zhu, Y. H., Zhu, Y. S., Lin, Q. X., et al., 2003. Characteristics of Early Jurassic Volcanic Rocks and Their Tectonic Significance in Haidewula, East Kunlun Orogenic Belt, Qinghai Province. *Earth Science—Jorunal of China University of Geosciences*, 28(6): 653–659 (in Chinese with English Abstract)